2D Physics-Based Deformable Shape Models: Explicit Governing Equations

Stelios Krinidis[†] and Ioannis Pitas[†]

[†]Aristotle University of Thessaloniki
Department of Informatics
Box 451
54124 Thessaloniki, Greece

Address for correspondence :
Professor Ioannis Pitas
Aristotle University of Thessaloniki
54124 Thessaloniki
GREECE
Tel. ++ 30 231 099 63 04
Fax ++ 30 231 099 63 04
email: pitas@zeus.csd.auth.gr

Abstract

This paper presents an accurate, very fast approach for the deformations of 2D physically based shape models representing open and closed curves. The introduced models overcome the main shortcoming of other deformable models, i.e. computation time. The approach relies on the determination of explicit deformation governing equations, that involve neither eigenvalue decomposition nor any other computationally intensive numerical operation. The approach was evaluated and compared with another fast and accurate physics-based deformable shape model, both in terms of deformation accuracy and computation time. The conclusion is that the introduced model is completely accurate and is deformed very fast on current personal computers.

Keywords

Deformable model, modal analysis, real-time deformations, finite element method, eigenvalue decomposition, deformable curves, governing equation.

Main Categories

Computer Animation and Virtual Humans (category 3)

I. Introduction

A key problem in machine vision is how to describe features, contours, surfaces, and volumes, so that they can be segmented, recognized, matched, or any other similar underlying process. The primary difficulties can be summarized as: a) object descriptions are sensitive to noise, b) objects can be nonrigid, and c) the shape of the 2D object projection varies with the viewing geometry. These problems have motivated the use of deformable models [1]-[5], to interpolate, smooth, and warp raw data, since these models provide reliable shape reconstruction tools that are both robust and generic.

The class of deformable shape models originates with the method of active contours ("snakes") introduced by Kass *et al.* [1], that are used to locate smooth curves in 2-D images. Since then, deformable models have been used for a number of applications in 2-D and 3-D by Terzopoulos, Witkin and Kass [6].

There have been two basic classes of deformable models: those based on parametric solid modelling primitives, such as those employed by Pentland *et al.* [2], and those based on mesh-like surface models, such as those in the work of Terzopoulos *et al.* [6]. In the case of parametric modelling, fitting has been performed using the "inside-outside" function of the modelling primitive [7], [8], whereas in the mesh surface models, a physical-motivated energy function has been employed [6], [9].

Both of these approaches are quite slow, requiring dozens of iterations in the case of parametric formulation, and up to hundreds of iterations in the case of physically-based mesh deformation. Hence, all the deformation-based approaches are too computationally intensive so as to achieve the desired results, since each intermediate step turns out to be extremely time-consuming. Thus, although finite elements are a powerful tool in computer vision applications, they are still computationally intensive when used to deform an object. We address this problem by introducing a 2D physics-based deformable approach representing open and closed curves, based on the finite element method (FEM), using explicit functions. Hence, a very fast approach is presented in this paper, involving only the calculation of an explicit function for the description of the deformations of the object under examination, as opposed to the eigenvalue decomposition that is necessary in most FEM approaches.

Our approach was motivated by the technique presented in [10], [11], which consists of analyzing nonrigid motion, with application to medical images. Nastar *et al.* [10] approximated the deforming object contour dynamically, using a physically based deformable curve/surface. In order to reduce the number of parameters describing the deformation, modal analysis, providing a spatial smoothing of the curve/surface, was exploited. On the same basis, we employed modal analysis and, after simplifying the deformation governing equations, we could safely infer that the deformations of open and closed 2D curves have explicit governing equations, involving neither eigenvalue decomposition nor any other computationally intensive operation.

The remainder of the paper is organized as follows. The 2D physics-based deformable shape models [10] are presented in Section II. In Section III the proof and the properties of the new deformable physics-based governing equations are introduced. A comparison between the initial deformation models [10] and the novel ones, are presented in Section IV, and final conclusions are drawn in Section V.

II. 2D Physics-Based Deformable Shape Modelling Based On Modal Analysis

In this Section, physically based deformable shape models [10], [11] exploiting modal analysis are introduced. We consider both the surface and volume properties of the objects at hand. We restrict ourselves to elastic deformations, i.e. we assume that the object recovers its original configuration as soon as all applied forces causing the deformation are removed.

Modelling an elastic 2D boundary can be achieved by an open or closed chain topology of N masses on the contour. Each model node has a mass m and is connected to its two neighbors with identical springs of stiffness k. The ratio $a = \frac{k}{m}$ constitutes the so-called *characteristic value* of the model, which is a constant value that describes the physical characteristics of the model. To be more detailed, it precisely determines the model's physical behavior. When a increases, the object tends to behave as a solid one, while when a decreases it can be treated as an elastic one.

The node coordinates of the model under examination are stacked in vector:

$$\mathbf{X}_0 = (x_1^0, y_1^0, \dots, x_N^0, y_N^0)^T \tag{1}$$

where N is the number of vertices (masses) of the chain. The parameters of the elastic properties of the model are needed (stiffness constant, dumping forces, external forces, etc.) for its full description [12]. The deformation of the model is governed by a differential matrix equation

[13]:

$$\mathbf{M}\ddot{\mathbf{U}} + \mathbf{C}\dot{\mathbf{U}} + \mathbf{K}\mathbf{U} = \mathbf{F} \tag{2}$$

where $\mathbf{U}$ is a vector storing nodal displacements of the initial circular chain $\mathbf{X_0}$. $\mathbf{M}, \mathbf{C}$, and $\mathbf{K}$ [12] are the mass, damping, and stiffness matrices of the model, respectively, and $\mathbf{F}$ is the force vector resulting from the attraction of the model by the object contour (usually based on the Euclidean distance between the object contour and the node coordinates). Equation (2) is a finite element formulation of the deformation process.

Instead of solving directly the equilibrium equation (2), one can transform it by a basis change:

$$\mathbf{U} = \mathbf{\Psi}\tilde{\mathbf{U}} \tag{3}$$

where $\mathbf{\Psi}$ is the square nonsingular transformation matrix of order N to be determined, and $\tilde{\mathbf{U}}$ is referred to as the *generalized displacement* vector. One effective way of choosing $\mathbf{\Psi}$ is setting it equal to $\mathbf{\Phi}$, a matrix whose entries are the eigenvectors of the generalized eigenproblem:

$$\mathbf{K}\boldsymbol{\phi_i} = \omega_i^2\mathbf{M}\boldsymbol{\phi_i} \tag{4}$$

$$\mathbf{U} = \mathbf{\Phi}\tilde{\mathbf{U}} = \sum_{i=1}^{N} \tilde{u}_i\boldsymbol{\phi_i} \tag{5}$$

Equation (5) is referred to as the modal superposition equation. The i-th column of $\mathbf{\Phi}$, denoted by ϕ_i, is the i-th vibration mode, $\tilde{u}_i$ (the i-th scalar component of $\tilde{\mathbf{U}}$) its amplitude, and ω_i its frequency. It should be noted that the vibration modes of a generalized eigenproblem involving real symmetric matrices can be chosen to be orthonormal vectors. Furthermore, using the standard Rayleigh hypothesis [10], matrices $\mathbf{K}$, $\mathbf{M}$ and $\mathbf{C}$ are simultaneously diagonalized:

$$\begin{cases} \mathbf{\Phi}^T\mathbf{M}\mathbf{\Phi} = \mathbf{I} \\ \mathbf{\Phi}^T\mathbf{K}\mathbf{\Phi} = \mathbf{\Omega}^2 \end{cases} \tag{6}$$

where $\mathbf{\Omega}^2$ is a diagonal matrix, whose elements are the frequencies ω_i^2 and $\mathbf{I}$ is the identity matrix.

In practice, we wish to approximate nodal displacements $\mathbf{U}$ by $\tilde{\mathbf{U}}$, which is the truncated sum of the M low-frequency modes, where $M \ll N$.

$$\tilde{\mathbf{U}} \approx \sum_{i=1}^{M} \tilde{u}_i\boldsymbol{\phi_i} \tag{7}$$

Vectors ϕ_i, $i = 1, \ldots, M$ form the *reduced modal basis* of the system. This is the major advantage of modal analysis: it is solved in a subspace corresponding to the M truncated low-frequency vibration modes of the deformable structure [2], [10], [11]. The number of vibration modes retained in the object description, is chosen so as to obtain a compact but adequately accurate representation. A typical *a priori* value for M, covering many types of standard deformations is equal to the quarter of the number of degrees of freedom of the system (i.e. 25% of the modes are kept).

An important advantage of this formulation is that the vibration modes (eigenvectors) and the frequencies (eigenvalues) of an open or closed chain topology have an explicit expression [10] and they do not have to be computed using slow eigen-decomposition techniques (due to the dimensions of matrices $\mathbf{K}$ and $\mathbf{M}$). The frequencies of the closed chain are given by:

$$\omega_i^2 = 4a\sin^2\left(\frac{\pi i}{N}\right) \tag{8}$$

and the vibration modes are obtained by:

$$\boldsymbol{\phi}_i = \left[\ldots, \cos\frac{2\pi ij}{N}, \ldots\right]^T \tag{9}$$

where $i \in \{1, 2, \ldots, N\}$ and $j \in \mathcal{B}(N)$. $\mathcal{B}(N)$ is the first Brillouin zone [10] and is equal to $\left\{-\frac{N}{2}+1, \ldots, \frac{N}{2}\right\}$ for N even, and $\left\{-\frac{N-1}{2}, \ldots, \frac{N-1}{2}\right\}$ for N odd. Furthermore, the case of an open chain topology is very similar, where the frequencies are given by:

$$\omega_i^2 = 4a\sin^2\left(\frac{\pi i}{2N}\right) \tag{10}$$

and the vibration modes are obtained by:

$$\phi_i = \left[\ldots, \cos\frac{2\pi(2i-1)j}{2N}, \ldots\right]^T \tag{11}$$

where $i \in \{1, 2, \ldots, N\}$ and $j \in [0, \ldots, N-1]$. Substituting (5) into (2) and premultiplying by $\mathbf{\Phi}^T$, (2) yields:

$$\ddot{\tilde{\mathbf{U}}} + \tilde{\mathbf{C}}\dot{\tilde{\mathbf{U}}} + \mathbf{\Omega}^2\tilde{\mathbf{U}} = \tilde{\mathbf{F}} \tag{12}$$

where $\tilde{\mathbf{C}} = \mathbf{\Phi}^T\mathbf{C}\mathbf{\Phi}$ and $\tilde{\mathbf{F}} = \mathbf{\Phi}^T\mathbf{F}$.

In many computer vision applications [11], when the initial and the final states are known, it is assumed that a constant force load $\mathbf{F}$ is applied to the body. Thus, equation (2) is called the equilibrium governing equation and corresponds to the static problem:

$$\mathbf{K}\mathbf{U} = \mathbf{F} \tag{13}$$

In the new basis, equation (13) is further simplified to $2N$ scalar equations:

$$\omega_i^2\tilde{u}_i = \tilde{f}_i \tag{14}$$

where ω_i designates the i-th frequency (eigenvalue) and the scalar $\tilde{u}_i$ is the amplitude of the corresponding vibration mode (corresponding to eigenvector $\boldsymbol{\phi_i}$). Equation (14), indicates that, instead of computing the displacements vector $\mathbf{U}$ from equation (13), we can compute its decomposition in terms of the vibration modes of the original chain.

The physical representation (final state) $\mathbf{X}(\tilde{\mathbf{U}})$ is finally found by applying the deformations to the initial circular chain:

$$\mathbf{X}(\tilde{\mathbf{U}}) = \mathbf{X}_0 + \mathbf{\Phi}\tilde{\mathbf{U}} \tag{15}$$

III. A Closed-Form Representation of the 2D Physics-Based Deformable Models

It is obvious that the deformations described above are still computationally intensive since they require the calculation of a large number of summations. In this Section our goal is to simplify the deformation process (Section II) and to introduce a new way of calculating the deformations, achieving very fast deformation computation, without loss of accuracy. As already mentioned, physics-based closed chain deformable model deformations $\boldsymbol{U}$ are described by:

$$U_i = \sum_j \frac{\sum_{n=1}^{N} [F_n \phi_n(j)]}{(1+\omega_j^2)\sum_{n=1}^{N} \phi_n^2(j)} \phi_i(j), \qquad j \in \mathcal{B}(N) \tag{16}$$

where $i \in \{1, 2, \ldots, N\}$, with N corresponding to the total number of nodes of the model, ω_i^2 is given by equation (8), $\phi_i(j)$ by equation (9), $\mathcal{B}(N)$ is the first Brillouin zone, and finally F_i denotes the x and y components of the force acting on node i:

$$\boldsymbol{F} = (F_{1_x}, F_{1_y}, F_{2_x}, F_{2_y}, \ldots, F_{N_x}, F_{N_y})^T \tag{17}$$

As it can be proved, the above equation for closed models is equivalent to:

$$U_i = \frac{1}{\sqrt{1+4a}} \sum_{j=1}^{N} F_j a^d \frac{\mu^{N-2d} + \lambda^{N-2d}}{\mu^N - \lambda^N} \tag{18}$$

The deformation governing equation for open chain physics-based deformable models is proved to be:

$$S_{i,j} = a^{|i-j|} \left[\mu^{2N-2|i-j|} + \lambda^{2N-2|i-j|}\right] \tag{19}$$

$$P_{i,j} = a^{i+j-1} \left[\mu^{2N-2(i+j-1)} + \lambda^{2N-2(i+j-1)}\right] \tag{20}$$

$$U_i = \frac{1}{\sqrt{1+4a}} \sum_{j=1}^{N} F_j \frac{S_{i,j} + P_{i,j}}{\mu^{2N} - \lambda^{2N}} \tag{21}$$

where μ and λ are two constant values equal to $\frac{\sqrt{1+4a}+1}{2}$ and $\frac{\sqrt{1+4a}-1}{2}$ respectively, a is the model's characteristic value, N is the total number of model nodes, and d is the distance (in nodes) between the node under examination and the node, where force F_i is applied. Hence, in practice, d (only for the closed models case) is equal to $min(|i-j|, |N-|i-j||)$.

For convenience, for the rest of the paper, our consideration will be focused on the closed physics-based deformable models. Thus, in practice, we wish to approximate nodal displacements $\mathbf{U}$ by $\tilde{\mathbf{U}}$, the truncated addition of the M' adjacent nodes, where $M' \ll N$:

$$\tilde{U}_i \approx \frac{1}{\sqrt{1+4a}} \sum_{j=i-M'}^{i+M'} F_j a^d \frac{\mu^{N-2d} + \lambda^{N-2d}}{\mu^N - \lambda^N} \tag{22}$$

The nodes i-M' to i+M', for each node i, form the *reduced nodal basis* of the system. This is the major advantage of the new form of the deformation governing equation: it is solved in a *nodal subspace* corresponding to the M' adjacent model nodes of the deformable structure [2], [10], [11]. The number of nodes retained, in the object description, for the calculations in each step is chosen so as to obtain a compact but adequately accurate contour representation. After performing a sequence of experiments it has been observed that a typical *a priori* value for M', covering many types of standard deformations, is equal to $\frac{\sqrt{1+4a}+1}{2} lnN$. Thus, only a very small number of adjacent nodes is taken into account in the calculations. This formulation is proved to be very fast, capable of use of real time applications.

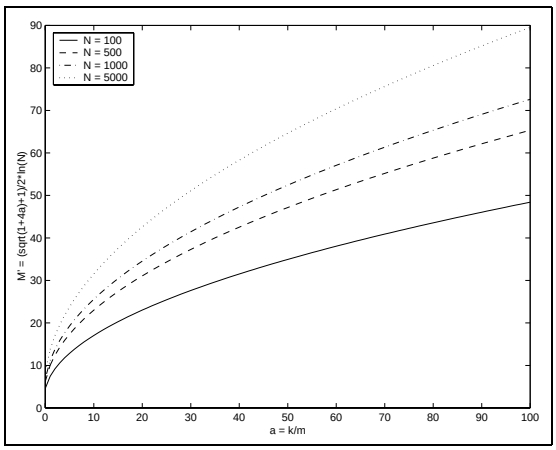

Fig. 1. *The relationship between model characteristic value a, and the nodal subspace M', with respect to the total number of model nodes N.*

IV. Performance Analysis of the Proposed Method

In this Section, a comparison between the initial physics-based deformable model using modal analysis (DMMA) described in Section II and the explicit formulation deformable model (EFDM) introduced in Section III is presented. The comparison is performed in terms of the displacement estimation error and the required computation time. The displacement error is defined as:

$$E = \frac{1}{N} \sum_{i} \left\| U_i - U_i' \right\| \tag{23}$$

where U_i and U_i' are the displacements calculated using DMMA (15) and the deformable model under comparison respectively. All experiments are performed on a Pentium III (700 MHz) workstation under Windows 2000 Professional without any particular code optimization.

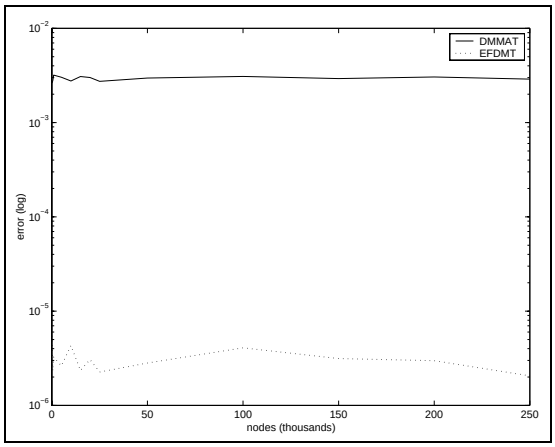

Fig. 2. ***Error comparison.*** *Errors regarding the modal and nodal reduction case respectively.*

The error comparison is illustrated in Figure 2. All errors in the Figure, are in a percentage form, due to the fact that the absolute error is not that representative, since it depends on the input forces applied to the model. The error difference of the EFDM and the DMMA is zero under any conditions. That is, the two equations, as expected, produce exactly the same results regardless of the deformable object characteristics a and the number of model nodes N. Furthermore, in Figure 2, one can see the errors of the initial deformable model in a reduced modal space (DMMAT), where only 25% of the eigenvalues are taken into account. The average error is 0.00293462%, which is insignificant. Thus, as Nastar *et al.* [10] claim, one can use the DMMAT without any particular loss of accuracy. Moreover, Figure 2 illustrates the errors for the introduced deformable physics-based model in a reduced nodal space (EFMDT), where only $\frac{\sqrt{1+4a}+1}{2} lnN$ adjacent (neighboring) nodes are considered. The average error is 0.00000314%, which is negligible with respect to the global deformation of the model, and consequently deformations can be computed using EFDMT without any particular loss of accuracy. Besides, it is clearly depicted in Figure 2 that deformations extracted from the EFDMT import an error 900 times less, in average, than the corresponding deformation computed by DMMAT. It must be noted that the errors do not change with the number of nodes N. Furthermore, note that error axis Y is a logarithmic one.

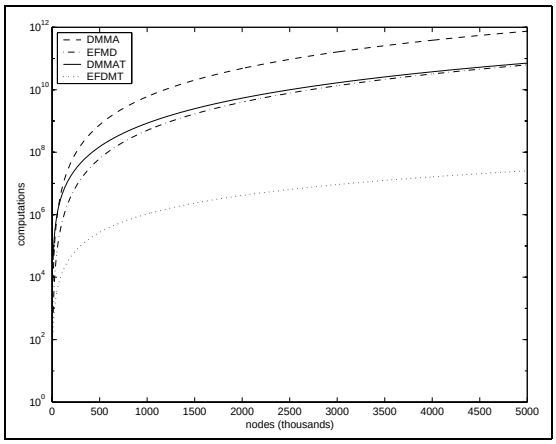

Fig. 3. ***Manual Computations.*** *Computations of the DMMA and DMMAT (25% of eigenvalues) have been manually estimated. The same task is performed for the EFDM and the EFDMT as well.*

Additionally, we have performed a computational complexity analysis of the methods under comparison. The DMMA (16) requires approximately $6N^3 + 14N^2$ computations (additions and multiplications, which are considered of equal complexity), where N is the number of model nodes. The simplified physics-based deformable model, EFDM, (eq. 18) requires only $\frac{1}{2}N^3 + \frac{7}{2}N^2$ computations. Thus, in theory, the explicitly calculated model has approximately 12 times fewer calculations than the initial one, for every N (Figure 3). However, the same task was performed for the DMMAT and the EFDMT. The corresponding computations are given by $\frac{1}{2}N^3 + 350N^2$ and $N^2 - NlnN(1 + lnN)$ respectively. These curves are plotted in Figure 3. It is worth noticing that the EFDMT has computational complexity of order $O(N^2)$, whereas the DMMAT has computational complexity $O(N^3)$.

Moreover, we have performed computation time benchmarking experimentally. Figure 4 shows the computation time for all methods under comparison. The

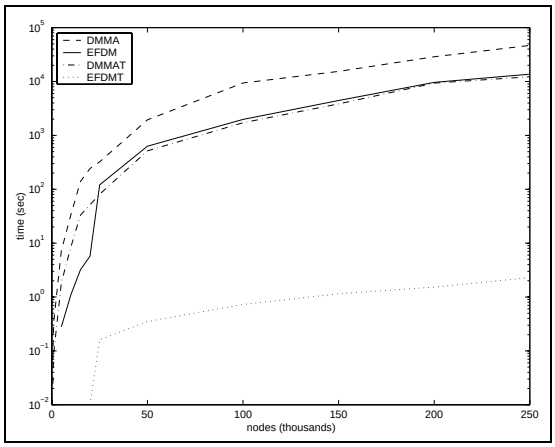

Fig. 4. ***Time comparison.*** *The EFDM compared with the DMMA with respect to computational time. The same task is performed for the DMMAT and the EFDMT. Times are measured in seconds.*

EFDM and DMMAT needs approximately the same computation time. This time is almost 3 times less than the corresponding time value of the DMMA. The computation times of these two cases are quite satisfactory, but they are still far from the desired e.g. for real time use which is achieved by EFDMT. It computes the deformations fast enough and only in the case the model nodes are more than 150.000, the computation time is more than 1 second. Therefore, that model can be deformed 100 times per second while having 20.000 nodes and $6,25$ times per second if it has 25.000 nodes. Hence, the EFDMT can be safely used in real time applications. Furthermore, it must be mentioned that in Figure 4 the computation times are plotted in a logarithmic axis for better visualization. In the cases of the EFDM and the DMMAT we have approximately equal computation time. The DMMA takes more computation time to achieve a result, whereas the EFDMT is much faster in performing the same deformation. We can achieve an acceleration of 4-5 orders of magnitude for almost any contour chain of length N. It must noted that the calculated execution speeds shown in Figure 4 are well in line with the comparing computational results shown in Figure 3.

V. Conclusion

In this article, we have presented a closed-form solution for 2D physics-based models deformation, along with their properties. Although all existing physics-based deformable models used in the literature, are a powerful tool in a number of computer vision applications, they are still computationally intensive when deforming an object. The presented 2D physics-based deformable model drastically reduces the computation time needed to perform the deformation. The deformation equations were simplified and analyzed. As a result, a closed-form solution can be reached for the objects deformation. This solution is very useful in analyzing the deformation behavior of the contour at hand.

The extremely low computational time and the low deformation error with respect to all the other available techniques in the literature, makes the introduced physics-based deformable model a very promising tool for various image analysis and computer vision applications.

References

[1] M. Kass, A. Witkin, and D. Terzopoulos. Snakes: Active contour models. *International Journal of Computer Vision*, pages 321–331, 1987.

[2] A. Pentland and S. Sclaroff. Closed-form solutions for physically-based shape modeling and recognition. *IEEE Transactions on Pattern Analysis and Machine Intelligence*, 13(7):730–742, 1991.

[3] D. Terzopoulos and D. Metaxas. Dynamic 3-D models with local and global deformations: Deformable superquadrics. *IEEE trans. Pettern Analysis and Machine Intelligence*, 13(7):703–714, July 1991.

[4] D. Terzopoulos, A. Witkin, and M. Kass. Constrains on deformable models: Recovering 3D shape and mon-rigid motion. *Artificial Intelligence*, 36:91–123, 1988.

[5] S. Sclaroff and A. Pentland. Modal matching for correspondence and recognition. *IEEE Transactions on Pattern Analysis and Machine Intelligence*, 17(6):545–561, June 1995.

[6] D. Terzopoulos, A. Witkin, and M. Kass. Symmetry-seeking models for a 3-D object reconstruction. *International Journal of Computer Vision*, 1(3):211–221, Oct. 1987.

[7] A. Pentland. Automatic extraction of deformable part models. *International Journal of Computer Vision*, 4(2):107–126, March 1990.

[8] F. Solina and R. Bajcsy. Recovery of parametric models from range images: The case for superquadrics with global deformations. *IEEE Transactions on Pattern Analysis and Machine Intelligence*, 12(2):131–147, 1990.

[9] K.Sobottka and I.Pitas. A novel method for automatic face segmentation, facial feature extraction and tracking. *Image Communication, Elsevier*, 12(3):263–281, June 1998.

[10] C. Nastar and N. Ayache. Frequency-based nonrigid motion analysis: Application to four dimensional medical images. *IEEE Transactions on Pattern Analysis and Machine Intelligence*, 18(11):1069–1079, 1996.

[11] C. Nikou, G. Bueno, F. Heitz, and J. P. Armspach. A joint physics-based statistical deformable model for multimodal brain image analysis. *IEEE Transactions on Medical Imaging*, 20(10):1026–1037, 2001.

[12] C. Nastar. *Models physiques deformables et modes vibratoires pour l'analyse du mouvement non-rigide dans les images multidimensionnelles*. Ph.D. Thesis, Ecole Nationale des Ponts et Chaussees, 1994.

[13] K. J. Bathe. *Finite Element Procedure*. Prentice Hall, Englewood Cliffs, New Jersey, 1996.